

# SHAPE ESTIMATION OF 3-D DNA MOLECULES FROM STEREO CRYO-ELECTRON MICRO-GRAPHS

*Mathews Jacob\**

Beckman Institute  
University of Illinois at Urbana-Champaign  
USA

*Thierry Blu, Michael Unser*

Biomedical Imaging Group  
Swiss Federal Institute of Technology  
Lausanne, Switzerland

## ABSTRACT

We introduce a 3-D parametric active contour algorithm for the shape estimation of DNA molecules from stereo cryo-electron micrographs. We consider a 3-D filament (consisting of a B-spline skeleton and a specified radial profile) and match its projections with the micrographs using an optimization algorithm. To accelerate the evaluation of the projections, we approximate the global model locally by an elongated blob-like template that is designed to be projection-steerable. This means that the 2-D projections of the template at any 3-D orientation can be expressed as a linear combination of a few basis functions. Thus, the matching of the template projections is reduced to evaluating a weighted sum of the inner-products between the basis functions and the micrographs.

We choose an internal energy term that penalizes the total curvature magnitude of the curve. We also use a constraint energy term that forces the curve to have a specified length. The sum of these terms along with the image energy obtained from the matching process is minimized using a conjugate-gradient algorithm. We validate the algorithm using real as well as simulated data.

## 1. INTRODUCTION

Cryo-electron microscopy is a technique used to image bio-molecules such as DNA. It uses a transmission electron microscope (TEM) to image specimens preserved in vitrous ice [1]. In this paper, we address the problem of the reconstruction of the 3-D shape of a DNA molecule from its stereo cryo-electron micrographs (a typical pair of such images is shown in Fig. 1). Since the exposure to electron beams causes the degradation of the specimen, one usually restricts the number of views to two. Due to physical constraints, the angular separation between the views is limited to a maximum of 30 degrees. The micrographs also suffer from poor image contrast and low SNR due to the low electron dose. All these aspects make the reconstruction problem difficult.

The early approaches to this problem included manual reconstruction [2] and a semi-automatic search algorithm called the flying cylinder [3]. The manual scheme is time-consuming and not necessarily reproducible. The flying cylinder algorithm detects the filament by matching the projections of a 3-D cylindrical template with the stereo images. The authors approximated the projections with oriented rectangles and used a sequential search algorithm to detect the filament fragments. These fragments were then sorted and interpolated to obtain a continuous curve. The performance of

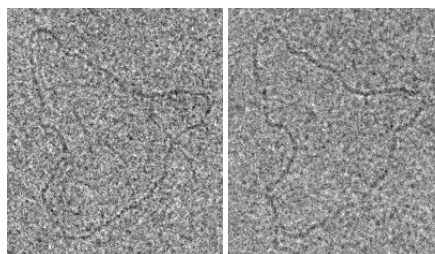


**Fig. 1.** Stereo views separated by  $30^\circ$  of a super-coiled DNA filament (1800 base pairs). Courtesy E. Larquet, Pasteur Institute, France.

this algorithm is limited by the approximations, angular discretization, and, the multi-step strategy.

We address these shortcomings and propose a new algorithm that solves the 3-D reconstruction problem in a more exact and consistent manner using projection-steerable templates and a 3-D active contour model. An outline of the full procedure is given in Fig. 2. We consider a global model for the DNA filament consisting of a 3-D parametric B-spline curve skeleton with a specified radial profile. Ideally, we would project the global model onto the projection planes and match the projections with the images to obtain a fitness measure. However, deriving the exact projections and matching them with the images in the optimization loop is computationally very expensive.

To reduce the computational complexity, we introduce the concept of projection-steerability, which is inspired by the work on 2-D orientation steerability by Freeman et. al. [4]. We then approximate the global 3-D model locally using elongated blob-like structures that are projection-steerable in the sense that their 2-D projections can be computed efficiently using a small number of appropriate basis functions. With this framework, the matching operation can be performed inexpensively as a weighted sum of the inner-products between the basis functions and the images. The weights are simple functions of the orientation of the 3-D template and the inner-products are evaluated efficiently by separable filtering. We discuss the projection-steerable ridge detection in detail in next section.

We derive a simple expression for the internal energy that penalize the total curvature magnitude of the curve, assuming it to be parametrized with a constant arc-length. Since the length of the DNA molecules are known a-priori, we use an additional constraint term that penalizes the curve for not having the specified length. We use a conjugate-gradient algorithm for snake optimization.

\*This research was supported by the Beckman Foundation and the Swiss National Science Foundation.

## 2. LOCAL FILAMENT DETECTION

In this section we deal with the detection of elongated blob-like structures from their stereo projections.

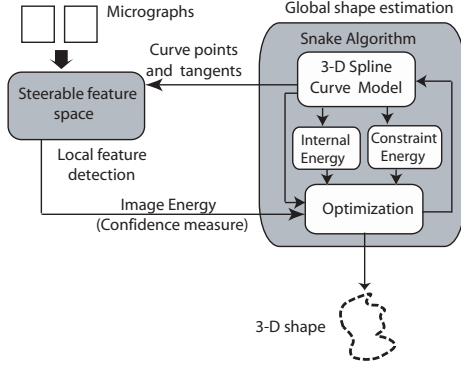


**Fig. 2.** Outline of the global 3-D shape estimation algorithm.

### 2.1. Projection-based feature detection

Suppose our task is to check for the presence of an elongated 3-D blob—denoted by  $f_c(\mathbf{r})$ ;  $\mathbf{r} \in \mathbb{R}^3$ —with an unknown orientation, at a particular position  $\mathbf{r}_c$  in a 3-D volume  $f$ . The volume is known only through its orthogonal 2-D projections  $f_i = \mathcal{P}_i f$ . We formulate the detection procedure as a matched filtering; we consider a 3-D detector and match its orthogonal projections onto the image planes with the micrographs.

We denote its rotated versions by  $h_{\mathbf{v}}(\mathbf{r}) = h(\mathbf{R}_{\mathbf{v}} \mathbf{r})$ , where  $\mathbf{R}_{\mathbf{v}}$  is a 3-D rotation matrix. We choose the sum of the inner-products between the 2-D template projections and the micrographs as the performance criterion:

$$C_{\mathbf{v}}(\mathbf{r}_c) = \sum_{i=0}^{N-1} \langle f_i, \mathcal{P}_i(h_{\mathbf{v}}) \rangle(\mathbf{r}_{c,i}) \quad (1)$$

$$= \sum_{i=0}^{N-1} (f_i * \mathcal{P}_i(h_{\mathbf{v}})^T)(\mathbf{r}_{c,i}) \quad (2)$$

where  $\mathcal{P}_i$ ;  $i = 0 \dots N-1$  are the orthogonal projection operators<sup>1</sup> and  $\mathbf{r}_{c,i} = \mathbf{P}_i \mathbf{r}_c$  is the projection<sup>2</sup> of  $\mathbf{r}_c$  onto the  $i^{\text{th}}$  image plane. Here  $h^T(\mathbf{r})$  denotes  $h(-\mathbf{r})$ . Note that the criterion is a function of the orientation vector  $\mathbf{v}$ . If we perform the filament detection independently at each point, the optimal orientation vector is the  $\mathbf{v}$  that yields the maximum of (1); the value of the maximum is a measure of the likeliness of the feature. However, the computation of the projections  $\mathcal{P}_i(h_{\mathbf{v}})$  are expensive for an arbitrary 3-D template; a direct implementation of the algorithm is not practical, unless simplifying assumptions are made.

<sup>1</sup>In our case  $N = 2$ , but the scheme is applicable for the general case as well.

<sup>2</sup> $\mathbf{P}_i = \mathbf{P}\mathbf{R}_i$ , where  $\mathbf{P} = \begin{bmatrix} 1 & 0 & 0 \\ 0 & 0 & 1 \end{bmatrix}$  and the unitary matrix  $\mathbf{R}_i$  specifies the projection geometry; it maps the co-ordinate system  $(x, y, z)$  onto  $(x_i, y_i, z_i)$ .

### 2.2. Projection-steerable ridge detection

To reduce the complexity in performing the projection matched filter detection, we use an approach similar to rotation-steerability [4]. We would like to have a good 3-D filament detector whose projections (for any spatial orientation) are contained in a space spanned by a few basis functions.

Let us consider the family

$$V_{3D} = \text{span} \{ \partial_{xx} g_3(\mathbf{r}; \sigma), \partial_{yy} g_3(\mathbf{r}; \sigma), \partial_{zz} g_3(\mathbf{r}; \sigma), \partial_{xy} g_3(\mathbf{r}; \sigma), \partial_{xz} g_3(\mathbf{r}; \sigma), \partial_{yz} g_3(\mathbf{r}; \sigma) \} \quad (3)$$

where  $g_D(\mathbf{r}; \sigma) = \frac{1}{(2\pi\sigma)^{\frac{D}{2}}} \exp\left(-\frac{|\mathbf{r}|^2}{2\sigma^2}\right)$  is a  $D$ -dimensional Gaussian and  $\partial_{xy} f(\mathbf{r}) = \frac{\partial^2}{\partial x \partial y} (f(\mathbf{r}))$ . We now show that any 3-D filter in this family is ideally suited for projection matched filter detection.

**Proposition 1** *The space  $V_{3D}$  is closed with respect to 3-D rotations.*

**Proof 1** *Since the Fourier transforms of the basis functions are second degree polynomials multiplied by a Gaussian window, the Fourier transform of a general function in this space is written as*

$$\hat{h}(\boldsymbol{\omega}) = (2\pi)^{\frac{3}{2}} (\boldsymbol{\omega}^t \mathbf{A} \boldsymbol{\omega}) g_3(\boldsymbol{\omega}; \sigma^{-1}) \quad (4)$$

*The Fourier transform of a  $\mathbf{R}$ -rotated version of  $h$  is given by*

$$\hat{h}(\mathbf{R}\boldsymbol{\omega}) = (2\pi)^{\frac{3}{2}} \left( \boldsymbol{\omega}^t \underbrace{\mathbf{R}^t \mathbf{A} \mathbf{R}}_{\mathbf{A}_{\mathbf{R}}} \boldsymbol{\omega} \right) g_3(\boldsymbol{\omega}; \sigma^{-1}), \quad (5)$$

*where  $\mathbf{R}$  is the 3x3 rotation matrix. This implies that  $\hat{h}(\mathbf{R}\boldsymbol{\omega}) \in V_{3D}$ .*

**Proposition 2** *The orthogonal projection  $\mathcal{P}_i$  of the space  $V_{3D}$  onto a plane is the function space  $V_{2D,i}$ :*

$$V_{2D,i} = \text{span} \{ \partial_{x_i x_i} g_2(\mathbf{r}_i; \sigma), \partial_{z_i z_i} g_2(\mathbf{r}_i; \sigma), \partial_{x_i z_i} g_2(\mathbf{r}_i; \sigma) \}. \quad (6)$$

**Proof 2** *The Fourier transform of the projection of an arbitrary function  $h(\mathbf{r}) \in V_{3D}$  is given by  $\hat{h}(\mathbf{P}_i^t \boldsymbol{\omega})$ :*

$$\hat{h}_i(\boldsymbol{\omega}_i) = \sqrt{2\pi} \left( \boldsymbol{\omega}_i^t \underbrace{\mathbf{P}_i \mathbf{A} \mathbf{P}_i^t}_{\mathbf{B}_i} \boldsymbol{\omega}_i \right) \underbrace{2\pi g_3(\mathbf{P}_i^t \boldsymbol{\omega}_i; \sigma^{-1})}_{g_2(\boldsymbol{\omega}_i; \sigma^{-1})}, \quad (7)$$

*where  $g_2$  is a 2-D Gaussian. Since the 2x2 matrix  $\mathbf{B}_i$  is symmetric,  $\hat{h}_i(\boldsymbol{\omega}_i)$  is a second degree polynomial in  $\boldsymbol{\omega}_i$ . This implies that  $h_i$  is a linear combination of the functions  $\partial_{xx} g_2(\mathbf{r}_i, \sigma)$ ,  $\partial_{xy} g_2(\mathbf{r}_i, \sigma)$  and  $\partial_{yy} g_2(\mathbf{r}_i, \sigma)$ . Thus  $\mathcal{P}_i(V_{3D}) \subseteq V_{2D,i}$ .*

*We also have the relations  $\mathcal{P}_i(\partial_{xx} g_3) = \partial_{x_i x_i} g_2$ ,  $\mathcal{P}_i(\partial_{zz} g_3) = \partial_{z_i z_i} g_2$  and  $\mathcal{P}_i(\partial_{xz} g_3) = \partial_{x_i z_i} g_2$ . They imply that  $V_{2D,i} \subseteq \mathcal{P}_i(V_{3D})$ . Thus we have  $V_{2D,i} = \mathcal{P}_i(V_{3D})$ .*

These results indicate that there is a very efficient way to rotate any function in  $V_{3D}$  and to compute its corresponding 2D projection using an appropriate weighted sum of basis functions. Hence, this class is ideally suited for projection-steerable matching.

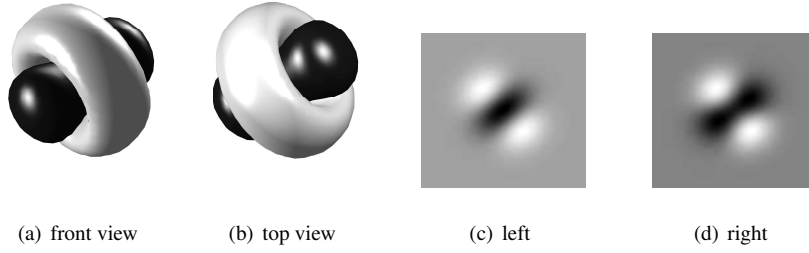


**Fig. 3.** (a) and (b) Isosurface plots of the front (viewed from the  $x$ - $z$  plane) and top (viewed from the  $x$ - $y$  plane) views of a 3-D detector oriented at  $30^\circ$  to the  $x$ -axis and  $30^\circ$  to the  $x$ - $y$  plane ( $\theta = 30^\circ, \phi = 30^\circ$ ). (c) and (d) Projections of the 3-D filter onto the image planes oriented at  $-15^\circ$  and  $-15^\circ$  to the  $y$  axis

### 2.3. 3-D ridge detection

We can show that the most elongated local template in  $V_{3D}$ , oriented along the vector  $\mathbf{v}$  is

$$h_{\mathbf{v}}(\mathbf{r}) = \underbrace{(\partial_{xx} + \partial_{yy} + \partial_{zz}) g_3(\mathbf{r}; \sigma)}_{\text{Laplacian of } g(\mathbf{r}; \sigma)} - \frac{5}{3} \partial_{\mathbf{v}\mathbf{v}} g_3(\mathbf{r}; \sigma), \quad (8)$$

where  $\partial_{\mathbf{v}\mathbf{v}} f(\mathbf{r}) = \frac{\partial^2}{\partial \gamma^2} f(\mathbf{r} + \gamma \mathbf{v})$ . We substitute (8) in (7) and perform some algebraic manipulations to obtain

$$\mathcal{P}_i(h_{\mathbf{v}}(\mathbf{r})) = \mathbf{v}^t [\mathbf{R}_i^t \mathbf{G}_i(\mathbf{r}_i; \sigma) \mathbf{R}_i] \mathbf{v}, \quad (9)$$

where  $\mathbf{G}_i(\mathbf{r}_i; \sigma)$  is the matrix

$$\begin{bmatrix} \partial_{z_i z_i} - \frac{2}{3} \partial_{x_i x_i} & 0 & -\frac{5}{3} \partial_{x_i z_i} \\ 0 & \partial_{x_i x_i} + \partial_{z_i z_i} & 0 \\ -\frac{5}{3} \partial_{x_i z_i} & 0 & \partial_{z_i z_i} - \frac{2}{3} \partial_{x_i x_i} \end{bmatrix} g_2(\mathbf{r}_i; \sigma). \quad (10)$$

This expression indicates that we use different 2-D detectors on the image planes, depending on the spatial orientation of the 3-D template. We give an example with the 3-D template and their projections in Fig. 3.

Using (9), we simplify (1) to

$$C_{\mathbf{v}}(\mathbf{r}) = \mathbf{v}^t \underbrace{\left[ \sum_{i=0}^{N-1} \mathbf{R}_i^t \mathbf{H}_{f_i}(\mathbf{r}_i) \mathbf{R}_i \right]}_{\mathbf{H}_{3D}(\mathbf{r})} \mathbf{v} \quad (11)$$

where  $\mathbf{H}_{f_i}(\mathbf{r}_i) = f_i * \mathbf{G}_i(\mathbf{r}_i; \sigma)$ . Thus, we can match the image locally with the projection of a 3-D blob oriented along  $\mathbf{v}$  by evaluating (11). To compute  $\mathbf{H}_{f_i}(\mathbf{r}_i)$  at every point in the micrograph, we need to filter the image with the templates corresponding to the 5 non-zero entries of (10). Since these entries are linear combinations of the three functions  $\partial_{x_i x_i} g_2(\mathbf{r}_i; \sigma)$ ,  $\partial_{z_i z_i} g_2(\mathbf{r}_i; \sigma)$  and  $\partial_{x_i z_i} g_2(\mathbf{r}_i; \sigma)$ , it is in fact sufficient to filter the images with three separable templates. The entries of  $\mathbf{H}_{f_i}(\mathbf{r}_i)$  are linear combinations of these filtered signals.

## 3. ACTIVE CONTOUR ALGORITHM

In this section, we discuss on the various energy terms of the snake algorithm.

### 3.1. Image Energy

The image energy term is a measure of the fit of the model to the image data. The tangent vector of the curve at a point  $\mathbf{r}(t)$ , given by  $d\mathbf{r}(t)$ , defines the direction of the elongated blob at that point. The likeliness of a blob at  $\mathbf{r}(t)$  oriented along  $d\mathbf{r}(t)$  can be computed using (11). The likeliness of the entire curve is obtained by integrating the goodness measures along the curve:

$$E_{\text{goodness}}(\mathbf{r}) = - \int_0^M d\mathbf{r}(t)^t \mathbf{H}_{3D}(\mathbf{r}) d\mathbf{r}(t) dt. \quad (12)$$

We maximize this measure to obtain the optimal B-spline representation of the skeleton; by doing so, we are jointly estimating the optimal orientations and magnitudes at the voxels through which the curve passes.

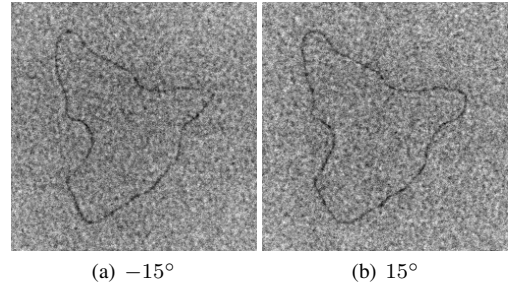


**Fig. 4.** Synthetic images used for the validation. They were generated from the manual reconstruction of Fig. 1 to generate the ground truth followed by simulating the image formation.

### 3.2. Internal Energy

The internal energy term is essentially a regularization term that penalizes non-smooth shapes, thus making the reconstruction problem better conditioned. The smoothness of the curve can be quantified by its total curvature magnitude. However, using this term directly as the internal energy leads to complicated expressions for the partial derivatives. Hence, we simplify this term to

$$\int_0^M |\kappa(\mathbf{r})|^2 dt = \frac{1}{c^2} \int_0^M |\mathbf{r}''(t)|^2 dt \quad (13)$$

which is valid if  $|\mathbf{r}'(t)|^2 = c$ ,  $\forall t$ ; that is, when the curve is parametrized by its curvilinear abscissa. To have this condition satisfied, we resample the user-initialized curve to have its knots placed uniformly along the curve.

	3-D Error	In-plane Error
Manual Tracing	$6.543 \pm 1.657$	$3.092 \pm 0.576$
Snake Output	$2.850 \pm 0.834$	$0.869 \pm 0.234$
Improvement	129.5%	258%

**Table 1.** Comparison with the reference curve for simulated micrographs: average value of the absolute error (in pixels).

### 3.3. External constraint energy.

The external constraint energy is a means for the user to enforce extra constraints on the reconstruction. We use two constraint terms in our implementation.

#### 3.3.1. Length constraint

The length of the DNA filaments are known a-priori; we introduce this information into the snake framework by penalizing the term

$$E_{\text{const}} = \left( \int_0^M |\mathbf{r}'(t)| dt - \text{Length} \right)^2, \quad (14)$$

where Length is the expected length of the molecule.

#### 3.3.2. Point constraint

We use a point constraint to enable the user to aid the reconstruction process; he can specify a few 3-D points that should lie on the final shape. The constraint energy is given by

$$E_{\text{const}} = \sum_{i=0}^{N_c-1} \min_{t \in [0, M]} |\mathbf{r}(t) - \mathbf{r}_{c,i}|^2, \quad (15)$$

where  $\mathbf{r}_{c,i}; i = 0, \dots, N_c - 1$  are the constraint points.

### 3.4. Optimization Algorithm

The algorithm begins with a user-initialized B-spline curve, which is then resampled to the constant arc-length parametrization. We use a conjugate-gradient optimization algorithm to derive the optimal parameters. Thanks to the projection-steerable formulation and the B-spline curve representation, the partial derivatives of the energy terms are computed exactly and efficiently.

## 4. EXPERIMENTS

In this section, we validate the snake algorithm using simulated data; we consider a 3-D curve (input by a user) and emulate the image formation. Some examples of generated micrographs are shown in Fig. 4.

To compare two 3-D curves  $C_a$  and  $C_b$ , we choose the error metric  $\mathcal{D}(C_a, C_b)$  as

$$\frac{1}{2} \left( \frac{1}{M_a} \int_0^{M_a} D(\mathbf{r}_a(t), C_b) dt + \frac{1}{M_b} \int_0^{M_b} D(\mathbf{r}_b(t), C_a) dt \right),$$

where  $C_a \equiv \mathbf{r}_a(t); t \in [0, M_a]$  and  $C_b \equiv \mathbf{r}_b(t); t \in [0, M_b]$ . The distance between a point  $\mathbf{r}_a(t)$  and a curve  $C_b$  (denoted in the above equation as  $D(\mathbf{r}_a(t), C_b)$ ) is defined as the distance between  $\mathbf{r}_a(t)$  and the closest point on  $C_b$ :

$$D(\mathbf{r}_a(t), C_b) = \min_{t' \in [0, M]} \|\mathbf{r}_a(t) - \mathbf{r}_b(t')\|_{L_2} \quad (16)$$

We evaluate the distance metric by discretizing both curves. We also look at the fit of the reconstruction with the available data. This measure (in-plane error) is the sum of the distances between the projections of the reconstructed curve and those of the reference curves.

We compared the performance of the snake algorithm with the manual tracing. We used 5 stereo pairs and 2 independent users. For each stereo-pair, we performed 5 manual tracings each. These tracings were used as the initialization for the snake algorithm. These tracings and the snake output were compared with the corresponding reference curves to obtain the absolute errors. The average errors in the manual tracings and the snake-fitted curves are given in Table I. Note that our algorithm gives a factor of 2.5 decrease in the in-plane errors. An example of the 3-D reconstruction using our algorithm is shown in Fig. 5.

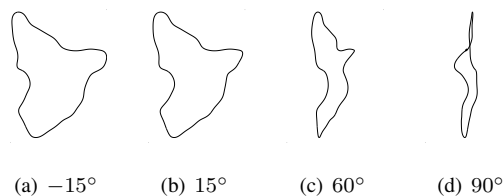


**Fig. 5.** Reconstructed filaments for the micrograph pair in Fig. 1 at different viewing angles around the vertical axis. (a) and (b) correspond to the left and the right micrographs in Fig. 1

## 5. CONCLUSION

We have presented a carefully engineered solution for the 3-D shape estimation of DNA molecules from stereo cryo-electron micrographs. We modeled the DNA filament as a structure with a 3-D B-spline curve skeleton and a specified radial profile. We optimized the B-spline coefficients using a conjugate-gradient algorithm such that the model projections match with the micrograph data. To make the algorithm computationally efficient, we use projection-steerable templates which reduces the matching process to the evaluation of a weighted sum. Starting from an user-initialized curve, the algorithm derives the optimal parameters using a conjugate-gradient algorithm. The results obtained are promising.

## 6. REFERENCES

- [1] J. Dubochet, M. Adrian, I. Dustin, P. Furrer, and A. Stasiak, "Cryoelectron microscopy of DNA molecules in solution," *Methods Enzymol.*, vol. 211, pp. 507–518, 1992.
- [2] I. Dustin, P. Furrer, A. Stasiak, J. Dubochet, J. Langowski, and E. Egelman, "Spatial visualization of DNA in solution," *Journal of Structural Biology*, vol. 107, pp. 15–21, 1991.
- [3] F. P. I. Margalef, P. Furrer, M. Kunt, and J. Dubochet, "The flying cylinder: A new algorithm for filament recognition in noisy stereo images," *Journal of Structural Biology*, vol. 116, pp. 25–29, 1996.
- [4] W. T. Freeman and E. H. Adelson, "The design and use of steerable filters," *IEEE Transactions on Pattern Analysis and Machine Intelligence*, vol. 13, no. 9, pp. 891–906, 1991.